actin moving assay on a microtubule bridge (*21*), a modification of the actin-bridge assay (*15*), by suspending a microtubule between two large beads immobilized on a glass surface to let the actin filament freely rotate in any direction. We found three swinging actin filaments that stayed primarily in the image plane and that were simultaneously translocated. All showed asymmetric swings (Fig. 4, fig. S6, and movies S5 and S6). When these filaments fluctuated, we saw moments when the filament became perpendicular to the image plane, appearing as a bright dot (red dotted frames in Fig. 4B; also Fig. 1C). Apparently the free neck could assume all orientations in space.

By attaching a micrometer-sized rod to a neck of the nanometer-sized molecular motor, we have been able to infer the neck motion continuously in real time. Viscous friction on the rod must slow down the motion, but essential features are likely preserved, as shown for the rotation of F_1-ATPase (*29*). The two necks of myosin V are connected via a free joint. Thus, the sole mechanism that can move a lifted head is Brownian rotation of the neck, but this is purely random, carrying the head in either direction with an equal probability. Ensuring forward landing thus requires a biasing mechanism(s). ATP-powered lever action of the landed neck, originally proposed for myosin II (*30*), moves forward the pivot of the Brownian rotation, producing the required bias, as has been suggested in electron microscopy and single-molecule studies (*16*, *19*, *26*, *27*). The rotational diffusion observed here implies that the lifted head stays off the actin surface for most of the time, as opposed to diffusional sliding of the myosin head along the actin surface (*31*). The rotational diffusion plus lever action, however, may not be sufficient. We have proposed that, to ensure forward landing of a lifted head in the presence of backward load, the track-binding surface of the head must be properly oriented such that forward swing of the neck makes the surface parallel with the track surface (*24*, *25*, *32*). One way to prove this orientational biasing experimentally is to attach a micrometer-sized rod. A rod that directly reports molecular orientations will be useful in studies where a conformational change in a protein machine, necessarily accompanying reorientation, is to be visualized during function.

References and Notes

1. K. Svoboda, C. F. Schmidt, B. J. Schnapp, S. M. Block, *Nature* **365**, 721 (1993).
2. R. D. Vale, *J. Cell Biol.* **163**, 445 (2003).
3. J. R. Sellers, C. Veigel, *Curr. Opin. Cell Biol.* **18**, 68 (2006).
4. R. S. Rock *et al.*, *Proc. Natl. Acad. Sci. U.S.A.* **98**, 13655 (2001).
5. S. Nishikawa *et al.*, *Biochem. Biophys. Res. Commun.* **290**, 311 (2002).
6. R. Mallik, B. C. Carter, S. A. Lex, S. J. King, S. P. Gross, *Nature* **427**, 649 (2004).
7. S. Toba, T. M. Watanabe, L. Yamaguchi-Okimoto, Y. Y. Toyoshima, H. Higuchi, *Proc. Natl. Acad. Sci. U.S.A.* **103**, 5741 (2006).
8. A. Yildiz *et al.*, *Science* **300**, 2061 (2003); published online 5 June 2003 (10.1126/science.1084398).
9. A. Yildiz *et al.*, *J. Biol. Chem.* **279**, 37223 (2004).
10. A. Yildiz, M. Tomishige, R. D. Vale, P. R. Selvin, *Science* **303**, 676 (2004); published online 18 December 2003 (10.1126/science.1093753).
11. S. L. Reck-Peterson *et al.*, *Cell* **126**, 335 (2006).
12. E. M. Espreafico *et al.*, *J. Cell Biol.* **119**, 1541 (1992).
13. R. E. Cheney *et al.*, *Cell* **75**, 13 (1993).
14. A. D. Mehta *et al.*, *Nature* **400**, 590 (1999).
15. M. Y. Ali *et al.*, *Nat. Struct. Biol.* **9**, 464 (2002).
16. M. L. Walker *et al.*, *Nature* **405**, 804 (2000).
17. J. N. Forkey, M. E. Quinlan, M. A. Shaw, J. E. Corrie, Y. E. Goldman, *Nature* **422**, 399 (2003).
18. E. Toprak *et al.*, *Proc. Natl. Acad. Sci. U.S.A.* **103**, 6495 (2006).
19. A. R. Dunn, J. A. Spudich, *Nat. Struct. Mol. Biol.* **14**, 246 (2007).
20. I. M. Crevel *et al.*, *EMBO J.* **23**, 23 (2004).
21. See supporting material on *Science* Online.
22. E. M. De La Cruz, A. L. Wells, S. S. Rosenfeld, E. M. Ostap H. L. Sweeney, *Proc. Natl. Acad. Sci. U.S.A.* **96**, 13726 (1999).
23. K. Kinosita Jr., S. Ishiwata, H. Yoshimura, H. Asai, A. Ikegami, *Biochemistry* **23**, 5963 (1984).
24. K. Kinosita Jr., K. Shiroguchi, M. Y. Ali, K. Adachi, H. Itoh, *Adv. Exp. Med. Biol.* **592**, 369 (2007).
25. K. Kinosita Jr., M. Y. Ali, K. Adachi, K. Shiroguchi, H. Itoh, *Adv. Exp. Med. Biol.* **565**, 205 (2005).
26. C. Veigel, F. Wang, M. L. Bartoo, J. R. Sellers, J. E. Molloy, *Nat. Cell Biol.* **4**, 59 (2002).
27. J. R. Moore, E. B. Krementsova, K. M. Trybus, D. M. Warshaw, *J. Cell Biol.* **155**, 625 (2001).
28. P.-D. Coureux, H. L. Sweeney, A. Houdusse, *EMBO J.* **23**, 4527 (2004).
29. R. Yasuda, H. Noji, M. Yoshida, K. Kinosita Jr., H. Itoh, *Nature* **410**, 898 (2001).
30. H. E. Huxley, *Science* **164**, 1356 (1969).
31. T. Okada *et al.*, *Biochem. Biophys. Res. Commun.* **354**, 379 (2007).
32. M. Y. Ali *et al.*, *Biophys. J.* **86**, 3804 (2004).
33. We thank M. Shio for designing a stable microscope stage, Y. Oguchi for help in myosin V purification, K. Adachi for an image analysis program, M. Fukatsu and K. Sakamaki for encouragement and lab management, and members of the Kinosita lab for discussions. Supported by Grants-in-Aid for Specially Promoted Research and the 21COE Program from the Ministry of Education, Sports, Culture, Science and Technology, Japan. K.S. was a Research Fellow of the Japan Society for the Promotion of Science.

Supporting Online Material
www.sciencemag.org/cgi/content/full/316/5828/1208/DC1
Materials and Methods
Figs. S1 to S6
Movies S1 to S6
References

26 January 2007; accepted 10 April 2007
10.1126/science.1140468

Hardwiring the Brain: Endocannabinoids Shape Neuronal Connectivity

Paul Berghuis,[1]* Ann M. Rajnicek,[2]* Yury M. Morozov,[3]* Ruth A. Ross,[2] Jan Mulder,[4] Gabriella M. Urbán,[5] Krisztina Monory,[6] Giovanni Marsicano,[6]† Michela Matteoli,[7] Alison Canty,[4] Andrew J. Irving,[8] István Katona,[5] Yuchio Yanagawa,[9] Pasko Rakic,[3] Beat Lutz,[6] Ken Mackie,[10]‡ Tibor Harkany[1]§

The roles of endocannabinoid signaling during central nervous system development are unknown. We report that CB_1 cannabinoid receptors (CB_1Rs) are enriched in the axonal growth cones of γ-aminobutyric acid–containing (GABAergic) interneurons in the rodent cortex during late gestation. Endocannabinoids trigger CB_1R internalization and elimination from filopodia and induce chemorepulsion and collapse of axonal growth cones of these GABAergic interneurons by activating RhoA. Similarly, endocannabinoids diminish the galvanotropism of *Xenopus laevis* spinal neurons. These findings, together with the impaired target selection of cortical GABAergic interneurons lacking CB_1Rs, identify endocannabinoids as axon guidance cues and demonstrate that endocannabinoid signaling regulates synaptogenesis and target selection in vivo.

In the cerebral cortex, information processing requires the precise temporal and spatial coordination of synaptic communication among excitatory pyramidal cells, inhibitory γ-aminobutyric acid–containing (GABAergic) interneurons, and subcortical afferents (*1*). Cortical neurons are born in progenitor zones that are distant from their final positions, and their layer-specific patterning is achieved through extensive migration in the developing cerebrum (*1*, *2*). En route to their destination, cortical neurons establish their synaptic connectivity patterns (*3*), thus providing the blueprint for their functional diversification.

In the adult central nervous system (CNS), presynaptic $\text{G}_{\text{i/o}}$ protein–coupled CB_1 cannabinoid receptors (CB_1Rs) (*4*) are the targets of marijuana (*Cannabis* spp.)–derived psychoactive phytocannabinoids and of the endocannabinoids anandamide (AEA) and 2-arachidonoylglycerol (2-AG). Endocannabinoids released from postsynaptic neurons serve as retrograde messengers that suppress neurotransmitter release at mature cortical synapses (*4*). During brain development, CB_1Rs are first expressed in early neural progenitors (*5*), with receptor levels increasing throughout neuronal specification and synaptogenesis (*6*). Although functionally active CB_1Rs are localized to developing axonal projections (*6*, *7*), it remains unknown whether endocannabinoids function as diffusible axon guidance factors before the growth cone differentiates into a presynaptic nerve terminal.

We defined the precise cellular distribution of CB_1Rs on neuronal precursors during cortical cell migration, axonal navigation, and synaptogenesis

Downloaded from www.sciencemag.org on February 26, 2015

by high-resolution laser-scanning microscopy of genetically tagged neurons, in situ hybridization, and electron microscopy (*3*, *8*). From embryonic day 13.5 (E13.5) until birth, CB_1Rs were present on pyramidal cells (Fig. 1, A to C) with their axons coursing in the intermediate zone of the developing cerebral cortex (*9*) (Fig. 1, D and E) and establishing the fornix pathway in the hippocampus (figs. S1 and S2). These projections primarily contained CB_1Rs associated with the surface of distal axon segments, with CB_1Rs being largely absent from their growth cones (Fig. 1F). In contrast, CB_1Rs were expressed in GABAergic interneurons during late gestation as they were undergoing intracortical tangential or radial migration (Fig. 1G). Here, CB_1Rs were preferentially found on axons and axonal growth cones (Fig. 1, H to J) coincident with establishing target-specific synaptic connectivity patterns (*3*, *10*).

CB_1R expression is spatially and temporally coordinated with endocannabinoid synthesis during brain development: *sn*-1-diacylglycerol lipases α and β (DAGLα/β), which synthesize 2-AG, predominated in elongating long-range telencephalic axons at around E14.5 (fig. S2) (*11*). By E18.5, however, DAGLα/β expression was localized to postsynaptic dendrites of glutamatergic pyramidal cells (Fig. 1, K to N), so that focal 2-AG release could control axonal growth cone steering and the formation of CB_1R^+ terminals (Fig. 1O). Postsynaptic DAGLα expression exceeded that of DAGLβ in the perinatal neocortex, in agreement with previous observations establishing DAGLα as the major postnatal DAGL isoform (*11*). Unexpectedly, the expression of *N*-acyl-phosphatidyl-ethanolamine-selective phospholipase D (NAPE-PLD), an enzyme participating in AEA synthesis (*4*), was delayed until E18.5, at which age NAPE-PLD was strongly associated with cortical pyramidal cells (Fig. 1, P and Q). GABAergic interneurons did not possess these endocannabinoid synthetic enzymes until their engagement in radial intracortical migration, coincident with the onset of postsynaptic target selection (Fig. 1R) (*3*).

To identify the functions of endocannabinoid signaling in axonal growth and guidance, we established GABAergic interneuron cultures with high CB_1R expression (*12*). Early growth cones of quiescent axons contained CB_1Rs localized to their leading filopodial tips (Fig. 2A). Morphological growth cone differentiation was associated with a gradual enrichment in CB_1Rs that were invariably present in motile filopodial tips at the leading edge of the growth cones (Fig. 2, B and C, and movie S1), which are critical for sensing guidance cues (*13*). Application of AEA for 15 to 30 min induced CB_1R translocation from filopodial tips to the central growth cone domain of GABAergic interneurons (Fig. 2, D and D′) and triggered receptor internalization and retrograde transport in hippo-

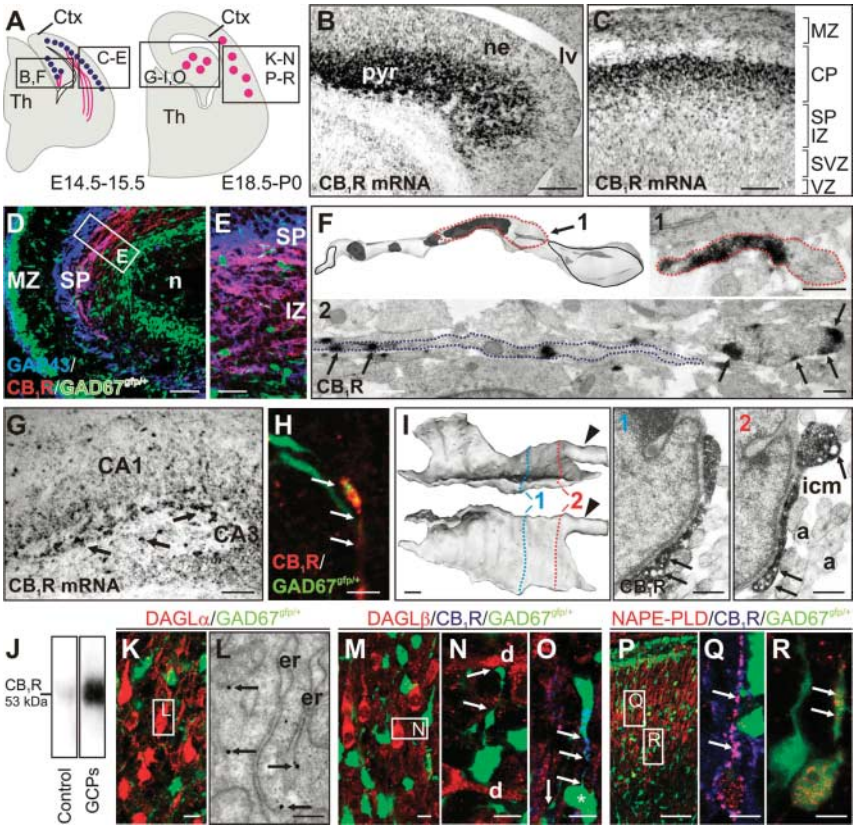

Fig. 1. The temporal and spatial coincidence of CB_1R localization with endocannabinoid availability during corticogenesis. (**A**) Schemes of the telencephalon at the embryonic days indicated. Colored symbols refer to particular structures in adjoining photomicrographs. At E14.5 to 16.5 (fig. S2B), CB_1R mRNA is preferentially expressed in pyramidal cells of the hippocampus (**B**) and cerebral cortex (**C**), with CB_1R immunoreactivity localized to developing long-range axons, coexpressing growth-associated protein 43 (GAP43), in the intermediate zone (*9*) (**D** and **E**). (**F**) CB_1R^+ processes, axons emitted by pyramidal neurons, in the fimbria. A three-dimensional reconstruction of a process is depicted in a semitransparent manner. A dotted line encircles the individual profile (1) shown to the right. (2) Adjacent CB_1R^+ processes (dotted line) with 3,3′-diaminobenzidine (DAB)–Ni reaction end products (black) precipitating on the inner plasmalemmal surface (arrows) after the use of an antibody recognizing the C terminus of CB_1R. (**G**) Hippocampal interneurons (arrows) express CB_1R mRNA at E18.5. (**H**) At birth, CB_1Rs are spatially associated with GABAergic axons (arrows) navigating locally in the hippocampus. (**I**) Reciprocally perpendicular projections of a single CB_1R^+ growth cone from the hilus of newborn rat hippocampus. Numbers indicate the positions of planar images. Arrowheads indicate the truncated axon. DAB precipitation fills the cytoplasm, which also contains numerous vesicles (arrows). (**J**) CB_1Rs concentrate in growth cone particles (GCPs) relative to total cortical lysates, as shown by Western analysis. (**K**) DAGLα predominates in the neocortex at birth and (**L**) is expressed by pyramidal cells. Arrows point to gold particles indicating the precise subcellular localization of DAGLα. (**M**) Similarly, DAGLβ is expressed by pyramidal cells in the neonatal cortex. (**N**) A putative GABAergic presynaptic bouton on a DAGLβ$^+$ dendrite is marked by arrows. (**O**) A CB_1R^+ GABAergic axon (arrows) is targeted toward a DAGLβ$^-$ interneuron (*) in the hippocampus at E18.5. (**P** and **Q**) NAPE-PLD is first expressed at E18.5 and is preferentially targeted to dendritic spines (arrows) in neocortical pyramids. (**R**) Some vertically migrating GABAergic interneurons possess NAPE-PLD expression. Arrows denote NAPE-PLD in the leading process. Abbreviations are defined in SOM text. Scale bars, 6 μm in (H), (K), (M) to (O), (Q), and (R); 50 μm in (E); 100 μm in (B) to (D), (G), and (P); and 500 nm in (F), (I), and (L).

---

[1] Division of Molecular Neurobiology, Department of Medical Biochemistry and Biophysics, Karolinska Institutet, S-17177 Stockholm, Sweden. [2] School of Medical Sciences, Institute of Medical Sciences, University of Aberdeen, Aberdeen Scotland AB25 2ZD, UK. [3] Department of Neurobiology, Kavli Institute for Neuroscience, Yale University School of Medicine, New Haven, CT 06510, USA. [4] Department of Neuroscience, Karolinska Institutet, S-17177 Stockholm, Sweden. [5] Laboratory of Cerebral Cortex Research, Institute of Experimental Medicine, Hungarian Academy of Sciences, H-1083 Budapest, Hungary. [6] Department of Physiological Chemistry, Johannes Gutenberg University Mainz, D-55099 Mainz, Germany. [7] Department of Medical Pharmacology and Consiglio Nazionale della Richerche Institute of Neuroscience, University of Milan, I-20129 Milan, Italy. [8] Neurosciences Institute, Division of Pathology and Neuroscience, Ninewells Hospital and Medical School, University of Dundee, Dundee, Scotland DD1 9SY, UK. [9] Department of Genetic and Behavioral Neuroscience, Gunma University Graduate School of Medicine and Solution Oriented Research for Science and Technology, Japan Science and Technology Corporation, Maebashi 371-8511, Japan. [10] Departments of Anesthesiology Physiology, and Biophysics, University of Washington, Seattle, WA 98195-6540, USA.

*These authors contributed equally to this work.

†Present address: U 862 Centre de Recherche François Magendie, INSERM, Equipe AVENIR 8 Université Bordeaux 2, 146 rue Léo Saignat, F-33077 Bordeaux, France.

‡Present address: Department of Psychological and Brain Sciences, Indiana University, Bloomington, IN 47405, USA.

§To whom correspondence should be addressed. E-mail: Tibor.Harkany@ki.se

campal neurons and PC12 pheochromocytoma cells recombinantly expressing CB$_1$Rs (fig. S3). Agonist-induced activation and trafficking of CB$_1$Rs translated into downstream signaling in cultured interneurons, because AEA (100 nM), like brain-derived neurotrophic factor (BDNF) (*14*), induced significant phosphorylation of Erk1 and Erk2 (Erk1/2) (*15*) in the central growth cone domain within 10 min (Fig. 2, E and E′). Studies in the growth cone particulate fraction isolated from embryonic rat cortices corroborated our in vitro findings by showing significant Erk2 phosphorylation that peaked 5 to 10 min after AEA (2 μM) application (Fig. 2F).

Direct involvement of chemotropic (endo) cannabinoid signaling in growth cone guidance was tested by assaying the growth cone turning responses of GABAergic interneurons induced by the synthetic CB$_1$R agonist WIN55,212-2 (*16*–*18*). A microgradient of BDNF, an established chemoattractive factor for GABAergic interneurons (*12*), induced attractive turning (*16*), whereas WIN55,212-2 at a concentration of 20 μM in the micropipette and ~200 nM at the growth cone (*16*) elicited growth cone repulsion (Fig. 3, A and B, and table S1). In $n = 13$ out of 20 motile growth cones (65%), WIN55,212-2 induced growth cone collapse and neurite retraction within the 60 min of recording (Fig. 3, A and B, and table S1). The lack of directional growth cone turning or neurite retraction in a control [dimethyl sulfoxide (DMSO)] gradient excluded recording artefacts produced by positive ejection pressure or the vehicle solution itself. Coapplication of the CB$_1$R antagonist AM251 (1 μM simultaneously in the pipette and bath solution) converted WIN55,212-2-induced chemorepulsion to attractive growth cone turning without significantly affecting the rate of neurite extension (Fig. 3B and table S1). Together with the lack of detectable CB$_2$ cannabinoid receptor expression in cultured GABAergic interneurons (*12*), these findings indicate that WIN55,212-2-induced chemorepulsion is mediated by CB$_1$Rs.

Next, we analyzed whether AEA and WIN55,212-2 modify directional growth cone steering of *Xenopus laevis* spinal neurons, which also express CB$_1$Rs (Fig. 3C). Growth cones steadily turned toward the cathode of a direct current (DC) electric field (EF) of 150 mV/mm (Fig. 3, D and E), a gradient that mimics the ~400 mV/mm DC-EF present naturally in the developing *Xenopus* neural tube (*19*) [supporting online material (SOM) text and fig. S4]. Bath application of either AEA or WIN55,212-2, but not its inactive stereoisomer WIN55,212-3, diminished both the mean angle turned toward the cathode and the frequency of cathodal turning in a dose-dependent fashion (Fig. 3, E and F, and table S1). Reminiscent of the ability of WIN55,212-2 to induce chemorepulsion (Fig. 3A), AEA or WIN55,212-2, but not WIN55,212-3, increased the frequency of EF-induced cathodal repulsion (anodal attraction) relative to vehicle controls (Fig. 3F).

Dynamic polarization of the growth cone cytoskeleton underlies chemotropism and galvanotropism: Extending microfilaments predominate on the side of the growth cone nearest to a chemoattractant source, whereas localized collapse of the actin cytoskeleton occurs near a repellent stimulus (*18*, *19*). Cytoskeletal integrity in axonal growth cones is controlled by members of the Rho family of small guanosine triphosphatases (GTPases) (*19*, *20*), which act as molecular switches that transduce extracellular stimuli to the actin cytoskeleton (*18*). Accordingly, WIN55,212-2 (2 μM) treatment selectively increased the GTP-bound active state of RhoA but not cumulative RhoA, -B, and -C activity (*20*) in primary cortical cultures after 5 min of stimulation (Fig. 4A). The involvement of CB$_1$Rs in this process was confirmed by the lack of RhoA activation in the presence of AM251 (2 μM; Fig. 4B). AEA (2 μM) induced RhoA activation in a manner similar to that of WIN55,212-2 (Fig. 4B). Spatially restricted activation of RhoA in the collapsing growth cone is associated with filopodial retraction and growth cone repulsion in response to chemical and electrical extracellular cues (*18*, *19*) through activation of the serine-threonine kinase Rho kinase (ROCK) and subsequent phosphorylation of myosin light chains (*19*, *21*) (fig. S5). Pretreating interneuron cultures with the ROCK-selective inhibitor Y-27632 (50 μM) (*18*) abolished WIN55,212-2-induced neurite retraction and converted CB$_1$R-mediated neurite repulsion into chemoattraction without significantly affecting the rate of neurite extension (Fig. 3, A and B, and table S1). The agonist-induced coupling of CB$_1$Rs to RhoA is

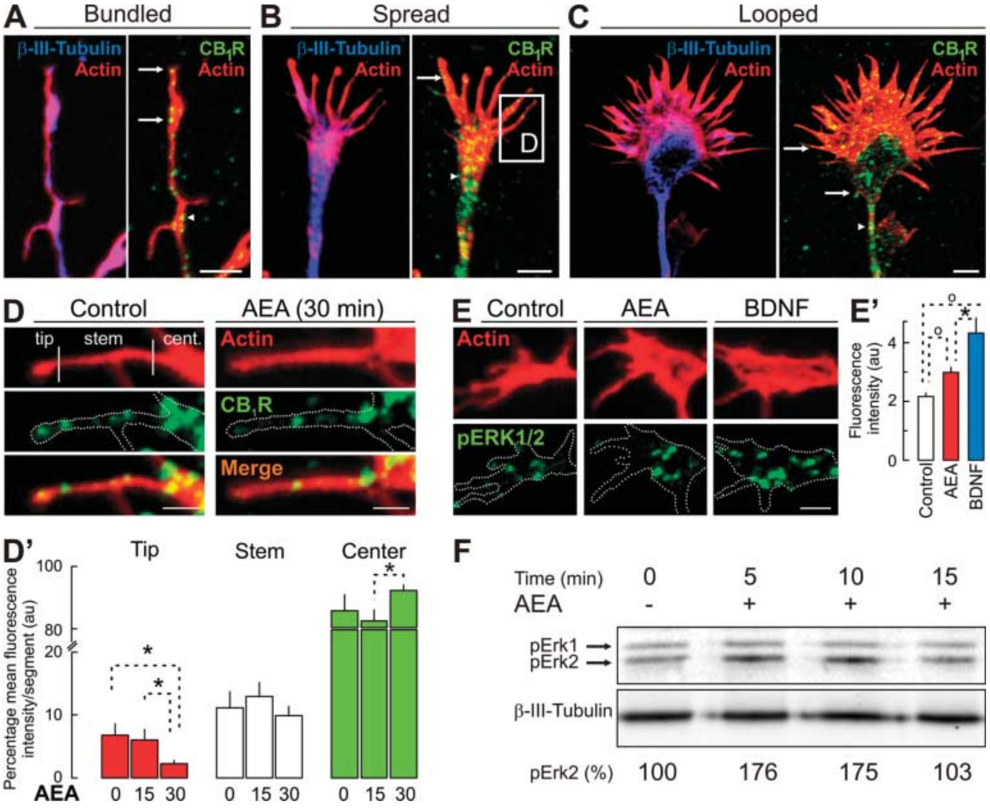

Fig. 2. Agonist stimulation induces CB$_1$R removal from filopodia and Erk1/2 phosphorylation in the central growth cone domain. (**A** to **C**) CB$_1$Rs are present in axonal growth cones of GABAergic interneurons in vitro. CB$_1$Rs are transported from the initial neurite segment through the neurite stem (arrowheads) to the growth cone, where they concentrate in filopodial tips (arrows) (movie S1). The structural classification of growth cones was based on whether microtubules in the central domain were bundled, spread, or looped (*29*). (**D** and **D′**) AEA (100 nM) induces CB$_1$R removal from filopodia. $^*P < 0.05$, $n = 13$ to 15 filopodia per group from two independent experiments. Numbers indicate the periods of AEA exposure, in minutes. (**E**) CB$_1$R activation induces Erk1/2 phosphorylation (pERK) in the central growth cone domain. (**E′**) Quantitative analysis of Erk1/2 phosphorylation 10 min after stimulation. $^{\circ}P < 0.01$, $^*P < 0.05$ ($n = 10$ growth cones per group). BDNF (100 ng/ml) was used as a positive control (*14*). (**F**) AEA induces Erk1/2 phosphorylation in growth cones isolated from embryonic rat cortices. β-III tubulin served as a loading control. Error bars represent SEM. Scale bars, 3 μm in (A) to (C), 2.5 μm in (E), and 1 μm in (D).

consistent with the concept that Rho family GTPases control growth cone integrity by stimulating contraction of the actin cytoskeleton on the side facing the repellent gradient, thus leading to growth cone collapse (*19*, *22*). The conversion of growth cone steering decisions upon ROCK inhibition suggests that CB_1Rs also activate the Cdc42 or Rac pathways, primary transducers of BDNF-induced chemoattraction (*18*, *20*), whose spatial and temporal antagonism with RhoA may be sufficient to switch (endo)cannabinoid-induced chemorepulsion to attractive turning (*18*).

We addressed the in vivo significance of the above findings in adult mice (4.5 to 6 months of age) lacking endocannabinoid-mediated retrograde signaling at cortical inhibitory synapses (*23*) because of conditional CB_1R deletion in GABAergic neurons by Cre-mediated recombination redirected by intergenic regulatory sequences of the genes *Dlx5* and *Dlx6* ($CB_1R^{f/f;Dlx5/6\text{-}Cre}$ mice) (*24*). We identified perisomatic GABAergic terminals that would otherwise have expressed CB_1Rs in the neocortex and hippocampus of $CB_1R^{f/f;Dlx5/6\text{-}Cre}$ mice by their coexpression of the vesicular GABA (VGAT) and vesicular glutamate 3 (VGLUT3) transporters (*25*, *26*) (Fig. 4C and fig. S6). Analysis of the distribution of $VGAT^+/VGLUT3^+$ boutons in layer 2/3 of the neocortex revealed a significant increase in the probability of pyramidal cells receiving $VGAT^+/VGLUT3^+$ inputs (Fig. 4, D to E′), indicating impaired postsynaptic target selection of cortical interneurons lacking CB_1R-mediated endocannabinoid signals. These changes occurred in the absence of altered interneuron migration or neurochemical specification (fig. S7).

Our findings outline an essential developmental role for endocannabinoid signaling in growth cone steering decisions, identifying endocannabinoids as a class of signaling molecules that regulate axon guidance. This function is evident in diverse CB_1R-expressing neuron populations as demonstrated in vitro by growth cone turning assays on CB_1R-expressing GABAergic interneurons in rodents and *Xenopus* spinal cord neurons. Our evidence that CB_1R-mediated endocannabinoid signals underpin growth cone steering by chemical and electrical extracellular directional cues, both of which are present in the embryonic CNS, suggests that endocannabinoid signals play an unexpectedly fundamental role in axonal pathfinding and neuritogenesis. The coincidence of intrinsic endocannabinoid synthesis in elongating long-range and GABAergic axons

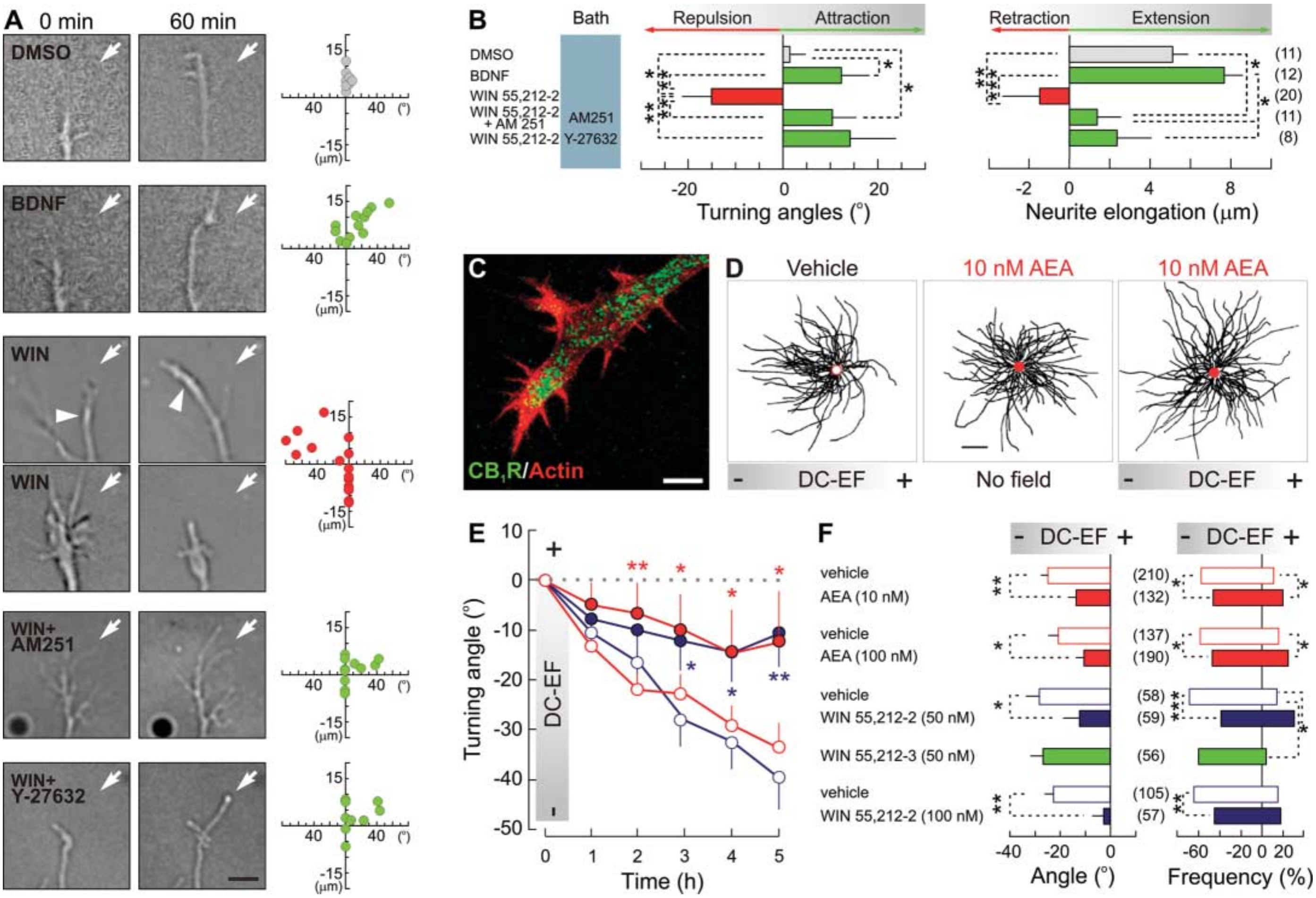

Fig. 3. CB_1R activation induces ROCK-dependent growth cone repulsion. (**A**) Neurites of cultured rodent GABAergic interneurons before and after 60 min of drug application. The microgradient direction is indicated by arrows. Arrowheads identify the neurites studied. Scatter plots show individual growth cone turning responses. Negative values represent neurite retraction. (**B**) Histograms of averaged growth cone turning responses in control and after drug treatments. Bath concentrations of the CB_1R antagonist AM251 and the ROCK-selective inhibitor Y-27632 were 1 μM and 50 μM, respectively (*18*). (**C**) Growth cones of *X. laevis* spinal neurons contain CB_1Rs. (**D**) Composite drawings of individual neurons at 3 hours were made by superimposing cell bodies at the colored dot, and the path of each neurite was traced. AEA inhibits growth cone turning toward the cathode in the DC-EF. (**E**) Time course of EF-induced growth cone turning. WIN55,212-2 (50 nM, solid blue circles) and AEA (100 nM, solid red circles) significantly inhibit cathodal growth cone steering over 5 hours in a continuous DC-EF, whereas growth cones in corresponding vehicle control cultures (open blue and red circles) turn increasingly toward the cathode. (**F**) The angle and frequency of cathodal growth cone turning (>10°) are each inhibited by both WIN55,212-2 and AEA but not by WIN55,212-3 after 3 hours. Negative angles indicate steering toward the cathode. Data represent means ± SEM. Sample sizes are indicated in parentheses. The statistical analysis is referred to in table S1. Scale bars, 4 μm in (A), 10 μm in (C), and 100 μm in (D).

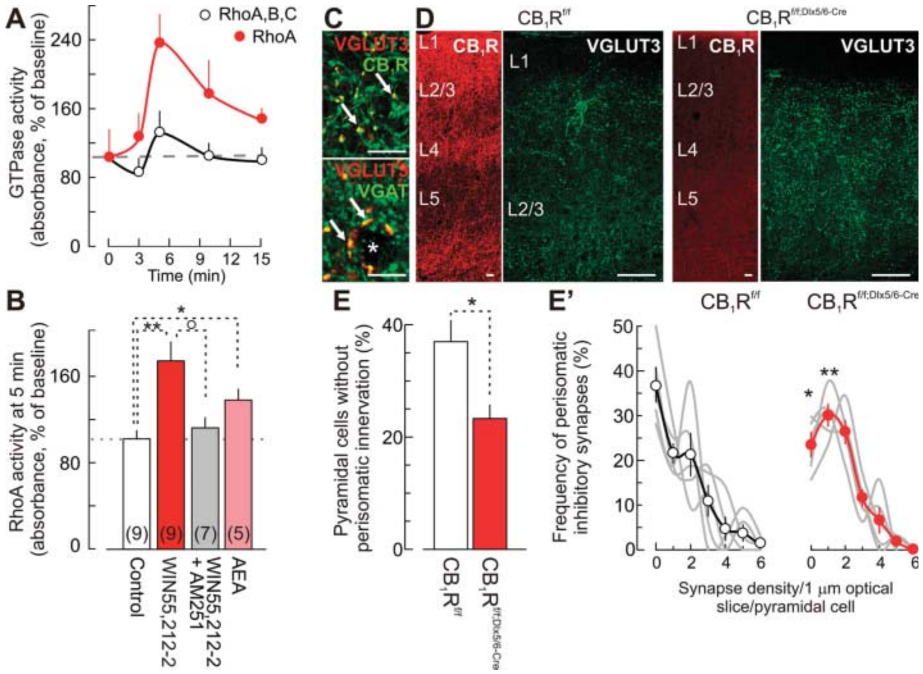

Fig. 4. The physiological importance of CB$_1$R-mediated growth cone repulsion. (**A**) Time course of WIN55,212-2 (2 μM)–induced Rho GTPase activation (n = 3 cortical cultures per data point from a representative experiment; mean ± SEM). (**B**) Both AEA and WIN55,212-2 activate RhoA through CB$_1$Rs, because this response is inhibited by pretreatment with AM251, a CB$_1$R antagonist. Sample sizes are given in parentheses (four independent experiments; mean ± SEM). $^{**}P = 0.008$, $^{*}P = 0.023$, $^{o}P = 0.014$. (**C**) In layer (L) 2/3 of the mouse somatosensory cortex, VGLUT3 labels inhibitory terminals of GABAergic basket cells (*25*) coexpressing CB$_1$Rs and VGAT (arrows). Asterisk denotes the pyramidal cell soma. (**D**) In CB$_1$R$^{f/f;Dlx5/6\text{-}Cre}$ mice (*23*), the lack of CB$_1$Rs in GABAergic interneurons is accompanied by the redistribution of VGLUT3-containing inhibitory afferents in L2/3. (**E** and **E′**) Cre recombinase–mediated CB$_1$R knockout leads to impaired postsynaptic target selection in CB$_1$R$^{f/f;Dlx5/6\text{-}Cre}$ mice, as indicated by the altered distribution and density of VGLUT3$^+$/VGAT$^+$-labeled perisomatic terminals on L2/3 pyramidal cells. Data are means ± SEM, $^{**}P = 0.024$, $^{*}P = 0.030$ (n = 5 mice per genotype, ≥32 cells per animal). Scale bars, 16 μm in (C) and 35 μm in (D).

demonstrates that autocrine endocannabinoid signaling (*11*) contributes to the initial growth of axons, whereas target-derived endocannabinoid signals control axonal navigation and positioning. Our conclusion is also supported by neuroanatomical findings showing endocannabinoid synthetic enzymes in cortical neurons coincident with the enrichment of CB$_1$Rs in neuronal growth cones during the critical period of postsynaptic target selection. Genetic evidence in CB$_1$R$^{f/f;Dlx5/6\text{-}Cre}$ mice (*24*) reveals that interneuron-specific deletion of CB$_1$R-mediated endocannabinoid signaling is sufficient to relieve the restriction of axonal elongation and branching (*12*), synaptogenesis (*27*), and target innervation mediated by endocannabinoid signals in neurochemically identified cortical interneurons. The present study also expands our understanding of how prenatal exposure to the CB$_1$R agonist Δ^9-tetrahydrocannabinol (THC), the major psychoactive constituent in cannabis, could affect CNS development and induce cognitive and behavioral deficits enduring into adolescence of THC-exposed offspring (*28*). Thus, our data, together with THC-induced impairment of synapse formation (*27*), imply that maternal marijuana consumption may affect neurodevelopment through sustained CB$_1$R activation and disrupt the proper positioning, postsynaptic target selectivity, and functional differentiation of developing axons.

References and Notes

1. P. Rakic, *Cereb. Cortex* **16** (suppl. 1), i3 (2006).
2. C. P. Wonders, S. A. Anderson, *Nat. Rev. Neurosci.* **7**, 687 (2006).
3. Y. M. Morozov, A. E. Ayoub, P. Rakic, *J. Neurosci.* **26**, 5017 (2006).
4. T. F. Freund, I. Katona, D. Piomelli, *Physiol. Rev.* **83**, 1017 (2003).
5. T. Aguado *et al.*, *FASEB J.* **19**, 1704 (2005).
6. X. Wang, D. Dow-Edwards, E. Keller, Y. L. Hurd, *Neuroscience* **118**, 681 (2003).
7. S. Mato, E. Del Olmo, A. Pazos, *Eur. J. Neurosci.* **17**, 1747 (2003).
8. Materials and methods are available as supporting material on *Science* Online.
9. A. R. Bicknese, A. M. Sheppard, D. D. O'Leary, A. L. Pearlman, *J. Neurosci.* **14**, 3500 (1994).
10. Y. M. Morozov, T. F. Freund, *Eur. J. Neurosci.* **18**, 1213 (2003).
11. T. Bisogno *et al.*, *J. Cell Biol.* **163**, 463 (2003).
12. P. Berghuis *et al.*, *Proc. Natl. Acad. Sci. U.S.A.* **102**, 19115 (2005).
13. T. P. O'Connor, J. S. Duerr, D. Bentley, *J. Neurosci.* **10**, 3935 (1990).
14. A. Patapoutian, L. F. Reichardt, *Curr. Opin. Neurobiol.* **11**, 272 (2001).
15. P. Derkinderen *et al.*, *J. Neurosci.* **23**, 2371 (2003).
16. G. X. Wang, M. M. Poo, *Nature* **434**, 898 (2005).
17. Y. Xiang *et al.*, *Nat. Neurosci.* **5**, 843 (2002).
18. X. B. Yuan *et al.*, *Nat. Cell Biol.* **5**, 38 (2003).
19. A. M. Rajnicek, L. E. Foubister, C. D. McCaig, *J. Cell Sci.* **119**, 1723 (2006).
20. A. B. Jaffe, A. Hall, *Annu. Rev. Cell Dev. Biol.* **21**, 247 (2005).
21. M. Amano *et al.*, *J. Biol. Chem.* **271**, 20246 (1996).
22. R. Kozma, S. Sarner, S. Ahmed, L. Lim, *Mol. Cell. Biol.* **17**, 1201 (1997).
23. M. R. Domenici *et al.*, *J. Neurosci.* **26**, 5794 (2006).
24. K. Monory *et al.*, *Neuron* **51**, 455 (2006).
25. T. Harkany *et al.*, *J. Neurosci.* **24**, 4978 (2004).
26. H. Hioki *et al.*, *Cereb. Cortex* **14**, 1266 (2004).
27. D. Kim, S. A. Thayer, *J. Neurosci.* **21**, RC146 (2001).
28. M. S. Spano, M. Ellgren, X. Wang, Y. L. Hurd, *Biol. Psychiatry* **61**, 554 (2007).
29. H. Morii, Y. Shiraishi-Yamaguchi, N. Mori, *J. Neurobiol.* **66**, 1101 (2006).

30. We thank M. Guzmán, Y. L. Hurd, G. Kunos, and M.-M. Poo for their critical comments; J. L. Rubenstein and M. Ekker for providing Dlx5/6-Cre mice; C. Ledent for CB$_1$R$^{-/-}$ colony founders; H. Hioki for antibody to VGLUT3; O. K. Penz for assistance with immunohistochemistry; K. M. Sousa for help with in situ hybridization; J. Bruce, H. Díack, and P. Wilson for assistance with galvanotropic turning assays; and A. Hubbard for high-resolution video microscopy. This work was supported by the Swedish Medical Research Council (T.H.); Stiftelsen Ragnhild och Einar Lundströms Minne (J.M. and T.H.); the Deutsche Forschungsgemeinschaft (B.L.); the Alzheimer's Association (K. Mackie and T.H.); the Ministry of Education, Culture, Sports, Science, and Technology of Japan (Y.Y.); the Ministry of Health, Labor, and Welfare of Japan (Y.Y.); Országos Tudományos Kutatási Alapprogramok (F046407, I.K.); Egészségügyi Tudományos Tanács (561/2006, I.K.); EUSynapse (M.M.); and NIH grants DA11322, DA015916, and DA00286 (K. Mackie). P.B. and I.K. are recipients of Hjärnfonden (Sweden) and János Bolyai (Hungary) scholarships, respectively. G.M.U. and I.K. were supported by the Howard Hughes Medical Institute and European Union contract LSHM-CT-2004-005166.

Supporting Online Material

www.sciencemag.org/cgi/content/full/316/5828/1212/DC1
Materials and Methods
SOM Text
Figs. S1 to S7
Table S1
References
Movie S1

10 November 2006; accepted 19 April 2007
10.1126/science.1137406

Hardwiring the Brain: Endocannabinoids Shape Neuronal Connectivity

Paul Berghuis *et al.*

Science **316**, 1212 (2007);
DOI: 10.1126/science.1137406

This copy is for your personal, non-commercial use only.

If you wish to distribute this article to others, you can order high-quality copies for your colleagues, clients, or customers by clicking here.

Permission to republish or repurpose articles or portions of articles can be obtained by following the guidelines here.

The following resources related to this article are available online at www.sciencemag.org (this information is current as of February 26, 2015):

Updated information and services, including high-resolution figures, can be found in the online version of this article at:
http://www.sciencemag.org/content/316/5828/1212.full.html

Supporting Online Material can be found at:
http://www.sciencemag.org/content/suppl/2007/05/22/316.5828.1212.DC1.html

A list of selected additional articles on the Science Web sites **related to this article** can be found at:
http://www.sciencemag.org/content/316/5828/1212.full.html#related

This article **cites 28 articles**, 16 of which can be accessed free:
http://www.sciencemag.org/content/316/5828/1212.full.html#ref-list-1

This article has been **cited by** 63 article(s) on the ISI Web of Science

This article has been **cited by** 46 articles hosted by HighWire Press; see:
http://www.sciencemag.org/content/316/5828/1212.full.html#related-urls

This article appears in the following **subject collections:**
Neuroscience
http://www.sciencemag.org/cgi/collection/neuroscience

Downloaded from www.sciencemag.org on February 26, 2015

Science (print ISSN 0036-8075; online ISSN 1095-9203) is published weekly, except the last week in December, by the American Association for the Advancement of Science, 1200 New York Avenue NW, Washington, DC 20005. Copyright 2007 by the American Association for the Advancement of Science; all rights reserved. The title *Science* is a registered trademark of AAAS.